IRREGULARITIES IN THE MOTION OF SPIN STABILISED EARTH SATELLITES

L. Fraiture N. Wiengarn B. Chambaz

European Space Operations Centre
(ESOC)
Darmstadt, W.-Germany

Applications Mathématiques & Logiciel
(AML)
Paris, France

ABSTRACT

This paper deals with small spin rate changes observed for rigid spinning spacecrafts. Spin rate variations can be caused by slowly moving internal parts. This has been studied in the context of METEOSAT 1. The periodic radiative albedo input may result in spin rate changes with the period of the orbit (near earth satellites) or diurnal variations (geostationary spacecraft). The first effect has been observed for ESRO IV while the latter is quantitatively verified for METEOSAT 1. We further investigate the long term spin rate change caused by the yearly thermal cycle of the satellite and compare it to the secular variation resulting from leaking thrusters. For the latter investigation the data of the geostationary satellite GEOS 1 are analysed.

1. INTRODUCTION

In this paper we consider the observed spinrate stability of rigid spinnning spacecrafts. Our attention goes in particular to effects of small magnitude which have been given little or no attention in the literature. Amongst others we exclude the analysis of nutation as well as spin rate decay due to eddy currents for near earth satellites. The observations we employ for this analysis come from three ESA spacecrafts : ESRO IV, a near earth scientific satellite, METEOSAT 1, a geosynchronous meteorological satellite quite similar to the US-SMS and GOES satellites and finally GEOS 2, a geosynchronous scientific satellite.

We consider three types of spin rate irregularities. The first is caused by slowly moving internal parts. The stepping motion over 18° in 25 min of the radiometer telescope of METEOSAT is the practical case we analyse. Concurrently, we provide a self contained theoretical explanation for the observed behaviour. The second type of irregularity consists of those variations which are periodic with the period of the orbit. For this case we present data of ESRO IV and METEOSAT 1. The latter is less subject to a mixture of influences and therefore a theoretical clarification is offered for the behaviour of this geostationary spacecraft. The analysis of the diurnal variation by P. Kohler (ref.6) has been simplified with respect to the satellite description and made more rigorous in tackling the Stefan-Boltzmann differential equation. The third and last type of variation is the secular spin up of GEOS 2. In fact a secular spin rate change in the same direction has often been observed. We attempt to explain this phenomenon by means of the 'leaking thruster' hypothesis.

1.1 Description of the satellites under study

To allow a better understanding of the context of the missions for which we have scrutinized the spin rate, we have added table 1. Masses and inertias are for the beginning of the routine payload operations. For METEOSAT 1 and GEOS 2 this means the early geosynchronous orbit phase.

1.1.1 METEOSAT 1. This spacecraft has been successfully launched on 23 November 1977. The nominal position at 0° longitude in geosynchronous orbit has been reached on 8 December 1977 and at the same day the scanning radiometer telescope has been put into operation. All the METEOSAT derived data presented in this paper have been taken during the first three months of operation.

Proc. Int. Symp. Spacecraft Flight Dynamics, Darmstadt, FRG, 18-22 May 1981 (ESA SP-160, Aug. 1981)

SATELLITE	TOTAL MASS	INERTIA RATIOS ALONG PRINC. AXES (KGM²)	TYPE OF ORBIT	NOMINAL SPINRATE	BOOMS
METEOSAT 1	280.6 kg	I_{XX} = 124.6 I_{YY} = 117.4 I_{SPIN} = 144.7	GEOSYNCHRONOUS 0° LONGITUDE ± 1° INCLINATION	100 rpm	NONE
ESRO IV	100.0 kg	I_{XX} = 13.5 I_{YY} = 13.5 I_{SPIN} = 15.0	NEAR EARTH = 239 = 1170 91.1° INCLINATION	65 TO 38 rpm	3 RIGID RADIAL BOOMS
GEOS 2	294.8 kg	I_{XX} = 310.4 I_{YY} = 165.3 I_{SPIN} = 404.5	GEOSYNCHRONOUS LONGITUDE ± 1° INCLINATION	10 rpm	2 RIGID RADIALS 2 RADIAL CABLES OF 20 EACH 4 AXIAL BOOMS

Table 1 : Synoptic data of the satellites studied.

Let us explain how the spin rate of METEOSAT 1 is sensed and computed. The satellite is equipped with two V-slit sun sensors. Each slit generates an electronic pulse when it crosses the sun. At the occasion of such a pulse, the contents of a running clock is copied in a register of 16 bits. This register is sampled every 0.7864 sec for every pulse type separately. The clock runs at 83333Hz and resets after 0.7864 sec. We call this 'parallel' sampling, because all pulses generated by various attitude sensors are recorded and transmitted during a basic sampling interval (here 0.7864 sec) or spin period whichever is the longest. At the control center a software preprocessor has to combine the relative pulse times to construct the spin rate and the other angular measurements. The METEOSAT attitude measurement preprocessor takes the telemetry format as the basis for an isolated spin rate estimate. Such a format lasts 25.17 sec and normally a mean over 3 to 16 first time differences for sun pulses inside a format is utilised. This leads to very accurate spin rates, i.e. quantization errors of $4.\ 10^{-3}$ rpm improved by the mean value and available every 25 sec.

1.1.2 ESRO IV. This near earth satellite was launched on 22 November 1972 and decayed after 17 months. During most of its life the spacecraft has gone through eclipses every orbit and the duration of these eclipses has been between 15 to 40 % of the orbital period. Thereby the satellite has undergone periodic thermal variations which have been very strongly reflected in the spin rate. To explain the spin rate modulation, a study contract has been placed with the "Compagnia Industriale Aerospatiale" in Rome and in 1975 Messrs. Buratti and Fusco (ref. 1) concluded the analysis. We only summarize their material with the intention to strengthen the experimental evidence for the intervention of earth albedo in observed spin rate modulations.

For the measurement of spin rates, the satellite has a meridian sun slit attached to a digital sunsensor. At every telemetry format start a 128 Hz counter is initiated and this counter is stopped before saturation if a sun pulse occurs within 1 sec. The recorded event is telemetered once every format (4.8 sec). Though larger gaps occur below 60 rpm, the spin rate obtained by this means in sunlit phases is quite accurate. In eclipse we can rely on the rotation of the earth magnetic vector measured inside the satellite. It is sensed by three perpendicular magnetometers and a skew one, all sampled at different times. The fact that the noisy magnetic field measurements projected on the spacecraft equator have to be fitted to a sine function with varying frequency makes it altogether cumbersome and much less accurate than the results derived from the sunsensor slit. Consequently the fine structure of the spin rate modulation in eclipse is lost in the noise. Therefore, the reported study (ref. 1) pays very little attention to the eclipse behaviour.

1.1.3 GEOS 2. This satellite was successfully launched on 15 July 1978. The fact that one of the scientific payloads is placed at the end of one of two 20 m long cable booms makes it in principle a flexible satellite. Flexible modes have relatively high frequencies. Unfortunately their analysis requires the accelerometer data. The accelerometers are parallel and skew parallel to the spin axis. The sampling of these data is via payload channels and can therefore only be performed at the occasion of particular events like the boom deployment or attitude and orbit manoeuvres. The optical sensors and the given sampling techniques are not adequate for studying short periodic variations of the spin rate which may be linked to flexibility. In the present study, we can assume that GEOS 2 is rigid because we will only use its data for a secular

spin rate variation analysis.

The measurement of the spin rate and the attitude angles for GEOS 2 is performed in 'series'. Only one measurement can be performed at one time and it consists of a predefined start and stop pulse combination (spin period, spin phase, sun colatitude and four combinations involving infrared sensors). A new measurement can only be taken if the previous one is telemetered. This means that a full cycle of 8 measurements can repeat at the earliest every 8 spin periods. At 10 rpm this is every 48 sec. The sampling and telemetering occurs every 1.38 sec and may thus increase the previous figure. The clock frequency during the count at 10 rpm in the geosynchronous orbit is 7937 Hz, leading to a possible quantisation of $4.2\ 10^{-4}$ rpm for an isolated spin rate. The GEOS 2 spin rate fluctuates strongly over one day.
The probable reason is the continuously changing power distribution situation required by the scientific payloads. This causes changes in the interior heat dissipation.

2. SPIN VARIATIONS DUE TO INTERNAL MOTION OF RIGID PARTS

For spinning spacecrafts, we can consider different kinds of internal motion. There can be light weight parts revolving quickly around some point, thus carrying momentum. If the rotational speed of such a part is constant, the total angular momentum of the spacecraft is biased by a fixed amount. We have no example for evaluation at hand and therefore we do not further discuss that case. Dual spin configurations have up to now not been flown by ESA and are therefore also excluded from our analysis.

The very slow step motion of a heavy and larger satellite part around a fixed axis inside the craft produces negligible momentum but influences the inertia tensor. This can be studied on METEOSAT 1 where the radiometer telescope and carriage jointly rotate over 18° in 2500 steps in 25 minutes. This section is entirely devoted to the evaluation of the spin disturbances in this case.

2.1.1 Inertia tensor changes. In this subsection we recall a few basic principles governing the inertias of composite rigid bodies. The aim is to find tractable approximations derived from rigorous dynamical and mathematical considerations. The generality with respect to the overall dynamical behaviour aspired to in the literature (ref. 9) is not available. A global and exact treatment does not suit our purpose, because we are looking for a perturbation of a nominal or reference behaviour. This reference motion is a perfect spin around a known axis. Assume that we have a prime body with mass m_1 (e.g. the satellite) to which a secondary rigid body with mass m_2 (e.g. the radiometer telescope) is attached at a given pivot point P.A body coordinate system (x_o, y_o, z_o) is defined inside the prime body and coincides with the principal moments of inertia of the total system if the secondary body is in the reference position. This

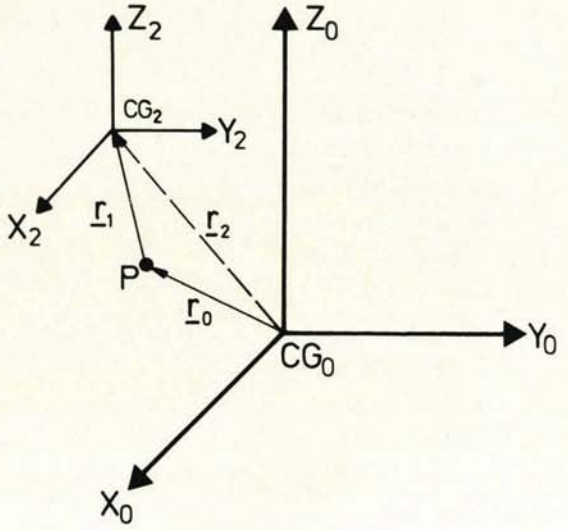

Figure 1

situation is depicted in Fig. 1. In the reference position, the center of gravity of the total system is in CG_o. By Steiner's rule, the inertia tensor of the total system can be constructed as follows

$$I^{tot} = J^{(1)} + J^{(2)} + I^{(2)} \qquad (2.1)$$

where $J^{(1)}$ and $J^{(2)}$ are the inertia matrices for the isolated main and secondary body, around CG_o and CG_2, respectively. The matrix $I^{(2)}$ contains the terms

$$i_{ll}^{(2)} = [(\underline{r}_2)_k^2 + (\underline{r}_2)_j^2]\, m_2$$
$$i_{kj}^{(2)} = (\underline{r}_2)_k\, (\underline{r}_2)_j\, m_2 \qquad (2.2)$$

for $k \neq l \neq j$. This corresponds to the inertia tensor around CG_o for the case that the mass of the secondary body is concentrated in CG_2.

It may be useful to say that in all what follows upper case characters are matrices, lower case characters are scalars except if they have an underline, where they stand for vectors. The components of a matrix are represented by lower case characters corresponding to the character used for the matrix itself, e.g. $j_{kl}^{(2)}$ belongs to $j^{(2)}$.

If the secondary body is rotated by a rotation R around some axis through the point P, then (2.1) can be rewritten as

$$I_o^{tot}(\theta) = J^{(1)} + RJ^{(2)}R^T + I^{(2)}(\theta) \qquad (2.3)$$

where T denotes transposition of the rotation matrix R. Here $I_o^{tot}(\theta)$ is the total inertia, not related to the center of gravity CG_θ of the new configuration but around the old center of gravity CG_o. The parameter θ represents a scalar rotation parameter which in most cases permits to set up R considering the nature of the constrained motion around P. The matrix $I^{(2)}(\theta)$ contains similar terms as defined by (2.2) but now $\underline{r}_2'(\theta)$ connects the new CG_θ with the CG_2 pivoted to a new position.

If we want to derive the actual new inertia tensor related to CG_θ we have to find CG_θ.

The position $\underline{r}_{cg}(\theta)$ of the CG_o in body coordinates can be found by making use of Fig. 2 where a fictitious not moving mass m_2 is put at $-\underline{r}_2(0)$. We see that

$$\underline{r}_{cg}(\theta) = \frac{m_1(\underline{r}_2(\theta) - \underline{r}_2(0))}{m_1 + m_2} \qquad (2.4)$$

and the distance of the secondary body to CG_o is

$$\underline{r}_2'(\theta) = \underline{r}_2(\theta) - \underline{r}_{cg}(\theta) \qquad (2.5)$$

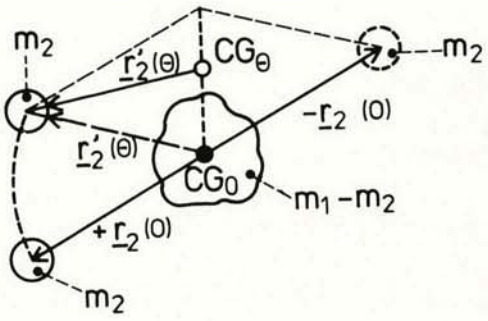

Figure 2

To obtain the inertia tensor of the composite body requires once more the application of Steiner's rule, or

$$I^{tot}(\theta) = I_o^{tot}(\theta) + I^{(1)}(\theta) \qquad (2.6)$$

where $I^{(1)}(\theta)$ contains the inertia of the main body concentrated in its center of mass with respect to CG_θ. If $m_2 << m_1$ and $||\underline{r}_2(\theta)||$ is small for all useful values of θ, the additional matrix $I^{(1)}(\theta)$ can be disregarded certainly in first order, and usually in second order approximations.

2.1.2 Second order development. Let us assume that we can develop $I^{tot}(\theta)$ in terms of θ and that $|\theta| << 1$ to ensure quick convergence, then we can write

$$I^{tot}(\theta) = I^{tot}(0) + \theta A + \theta^2 B + \mathcal{O}(\theta^3) \qquad (2.7)$$

In the beginning of this subsection, we have assumed that $I^{tot}(0)$ is diagonal by putting x_o, y_o and z_o on the principal axes. Thus, we can say

$$i_{kl}^{tot}(0) = \lambda_k \delta_{kl} \qquad (2.8)$$

The coordinate axes along x_o, y_o and z_o are denoted by $\underline{e}_1$, $\underline{e}_2$ and $\underline{e}_3$ respectively. Hence, to the second order, the eigenvalue approximation is given by

$$[I^{tot}(0) + \theta A + \theta^2 B]\ [\underline{e}_i + \theta \underline{f}_i + \theta^2 \underline{s}_i]$$

$$= [\lambda_i + \theta c_i + \theta^2 d_i]\ [\underline{e}_i + \theta \underline{f}_i + \theta^2 \underline{s}_i] \qquad (2.9)$$

as suggested by Kato (ref. 5). For obvious reasons, the correction $\underline{f}_i$ and $\underline{s}_i$ to the zero-th order eigenvector can only be perpendicular to the latter. Thus, $\underline{e}_i^T \underline{f}_i = \underline{e}_i^T \underline{s}_i = 0$ is true for all i. Further we assume that $\underline{e}_i$ is a unit vector.

Limiting ourselves to the first order, we see that the unknowns involved in (2.9) are the two non-zero components of $\underline{f}_i$ and the scalar c_i. Working out (2.9) without second order yields

$$I^{tot}(0)\underline{f}_i + A\underline{e}_i = c_i \underline{e}_i + \lambda_i \underline{f}_i \qquad (2.10)$$

which for a given i represents three linear equations in three unknowns. The solutions are

$$c_i = a_{ii} \qquad (2.11)$$

$$(\underline{f}_i)_j = \frac{a_{ij}\,(1 - \delta_{ij})}{\lambda_i - \lambda_j} \qquad (2.12)$$

where δ_{ij} is the Kronecker delta.

Having the first oder quantities at our disposal, we can find the three second order scalars in $\underline{s}_i$ and d_i from

$$I^{tot}(o)\underline{s}_i + A\underline{f}_i + B\underline{e}_i = \lambda_i \underline{s}_i + c_i \underline{f}_i + d_i \underline{e}_i \qquad (2.13)$$

They are

$$d_i = b_{ii} + \sum_{k=1}^{3} \frac{a_{ik}^2}{\lambda_i - \lambda_k}\,(1 - \delta_{ik}) \qquad (2.14)$$

and

$$(\lambda_i - \lambda_j)\,(\underline{s}_i)_j = b_{ij} + \frac{a_{ik}a_{jk}}{\lambda_i - \lambda_k} + \frac{(a_{jj} - a_{ii})a_{ij}}{\lambda_i - \lambda_j} \qquad (2.15)$$

where b_{ij} and $(\underline{s}_i)_j$ are again elements of B and $\underline{s}_i$, respectively. In (2.15) the indices i, j, and k are strictly different.

2.1.3 Spin changes. We make the convention that $\underline{e}_3$ is along the nominal or reference spin axis (θ=0). Then c_3 and d_3 decide on the spin rate change $\Delta\omega(\theta)$ with respect to a reference spin rate ω. Due to the conservation of kinetic momentum in the absence of external torques, we can write for nutation free motion

$$\Delta(i_{33}\omega) = 0 \qquad (2.16)$$

up to the second order, we can formally represent the spin rate as

$$\omega = \omega_o + \theta\Delta\omega_1 + \theta^2\Delta\omega_2 + \mathcal{O}(\theta^3) \qquad (2.17)$$

By strictly applying (2.16) and taking into account that it must be true for any small θ, we obtain

$$\frac{c_3}{\lambda_3} = -\frac{\Delta\omega}{\omega_o}\,\frac{1}{} \qquad (2.18)$$

and

$$\frac{\Delta\omega_1}{\omega_o}\,\frac{c_3}{\lambda_3} + \frac{\Delta\omega_2}{\omega_o} = -\frac{d_3}{\lambda_3} \qquad (2.19)$$

Let us now turn to the spin axis tilt. By tilt we mean the angle by which the actual spin axis moves away from its reference position it occupies in the body if $\theta = 0$. The spin axis tilt directly influences the sun colatitude measurement and causes a north-south deformation of the meteorological image taken by the moving radiometer telescope.

From the previous subsection we know that the eigenvector $\underline{e}_z$ which is located on the z-axis if $\theta = 0$, becomes

$$(\underline{e}_z)_x = (\underline{f}_3)_1\theta + (\underline{s}_3)_1\theta^2 + \mathcal{O}(\theta^3)$$

$$(\underline{e}_z)_y = (f_3)_2\theta + (\underline{s}_3)_2\theta^2 + \mathcal{O}(\theta^3)$$

$$(\underline{e}_z)_{zz} = 1 \qquad (2.20)$$

for non zero θ. It should be stressed that $\|\underline{e}_z\|$ is different from unity if $\theta \neq 0$. This corresponds to two small rotations η_x and η_y around the x and y-axes, respectively. We have

$$\sin \eta_x \simeq \eta_x = \frac{(e_z)_y}{\sqrt{1+(e_z)_y^2+(e_z)_x^2}} \simeq$$

$$(e_z)_y + (\eta^3) + (\theta^3) \quad (2.21)$$

and approximating in the same way

$$\eta_y \simeq (e_z)_x + \mathcal{O}(\eta^3) + \mathcal{O}(\theta^3) \quad (2.22)$$

if θ, η_x and η_y are all small.

2.2 Application to METEOSAT

The information of the mechanical detail of the design of METEOSAT 1 which reached the authors is rather poor. We quote two technical documents (ref. 2) and ref. 3). These allow to draw fig. 3. The pivot point P at rest should coincide with the CG_o of the total satellite in the reference position. We further assume that the carriage mass is sufficiently concentrated around its CG, so that its own inertia tensor has a negligeable effect on the whole. Carriage and telescope are forced to move together around the pivot point in 2500 steps over 18° during 25 min. Five further minutes are reserved for a quick retrace and damping of nutation. The effect of this stepping and retrace on the spin rate is displayed in figure 4. This graph is obtained by superposition of many intervals and shows a mean value and the quantisation error limits obtained from the actual flight data.

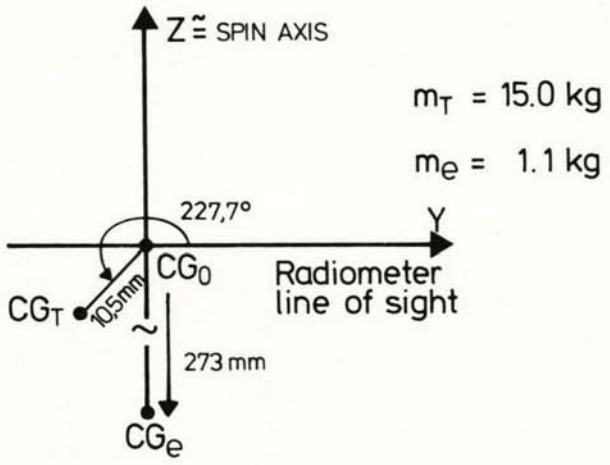

Figure 3

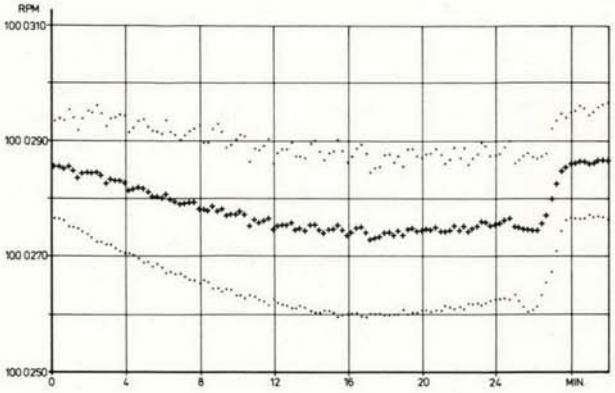

Figure 4

Let us assume that the configuration in Fig. 3 is the reference, or that θ moves from + 9° to - 9° around it. In a quick calculation on the motion of the CG of the whole satellite for these extremes, we find that it is at most 1 mm in the y-direction and one order of magnitude smaller in the z-direction. Thus we can neglect the shift of the CG and refer to (2.1). In the METEOSAT case this formula implies the following matrix terms for the total inertia tensor if $j \neq k \neq 1$

$$i_{ll}^{tot}(=0) = j_{ll}^{(1)} + j_{ll}^{(T)} + m_T((x_j^T)^2 + (x_k^T)^2) + m_c((x_j^c)^2 + (x_k^c)^2) \quad (2.23)$$

and

$$i_{kl}^{tot}(\theta=0) = j_{kl}^{(1)} + j_{kl}^{(T)} - m_T(x_k^T)(x_l^T) - m_c(x_k^c)(x_l^c) \quad (2.24)$$

where the superscript (1) refers to the satellite without moving parts, (T) means telescope and 'c' stays for carriage. To compress the notation we have introduced $x_1=z$, $x_2=y$ and $z_3=z$ as coordinates in the satellite body system.

The next step consists in working out (2.3) assuming a rotation matrix $R_x(\theta)$ representing a rotation θ around x_1 expanded to the second order. We further know that $x_1^c = x_1^T = 0$, i.e. the motion is in the y-z-plane. Say that $\alpha = \cos(227.7^o)$ and $\beta = \sin(227.7^o)$ then

$$x_2^c \simeq r^c\theta \qquad ; \; x_3^c \simeq r^c(1 - \frac{\theta^2}{2})$$

$$x_2^T \simeq r^T(\alpha - \beta\theta - \frac{\alpha}{2}\theta^2)$$

$$x_3^T \simeq r^T(\beta + \alpha\theta - \frac{\beta}{2}\theta^2)$$

2.2.1 The spin rate variation. We are now in a position to derive the matrices A and B defined in (2.7). For the spin rate (2.20) we need $c_3 = a_{33}$ and d_3 in (2.14) requiring b_{33}, a_{13}, and a_{23}. The substitution into (2.3) of the approximations just made yields :

$$a_{33} = -2j_{23} + m_T r_T^2 (- 2\alpha\beta)$$

$$b_{33} = j_{22} - j_{33} + m_T r_T(\beta^2 - \alpha^2) + m_c r_c^2$$

$$a_{13} = - j_{13}$$

$$a_{23} = - (j_{22} - j_{33}) + j_{23} + m_T r_T (\beta^2 - \alpha^2) + m_c r_c^2$$

Let us now introduce the numerical data. We have

$$j_{33}^{(T)} - j_{22}^{(T)} = 0.143 \pm 1.6 \; 10^{-3} \; kgm^2$$

$$j_{23}^{(T)} = (1.24 \pm 1.6) \; 10^{-3} \; kgm^2$$

while we miss the other information on $^{(T)}$. From figure 3 we further derive that

$$2 \, m_T r_T^2 \alpha\beta = 2.15 \; 10^{-3}$$

and

$$m_T r_T^2(\beta^2 - \alpha^2) + m_c r_c^2 = 0.0822$$

Combining these figures leads to the following values

$$c_3 = a_{33} = -(4.63 \pm 3.2) \; 10^{-3}$$

$$b_{33} = -0.061 \; ; \; a_{23} = 0.226$$

while for $a_{13} = -j_{12}^{(T)}$ we have nothing specific to offer; we will just assume that it is negligible.

According to table 1 the $\lambda_3 = I_{spin} = 144.7$, and in virtue of (2.19) we find

$$(\frac{\Delta\omega_1}{\omega_o})_{theory} = (3.2 \pm 2.2) \; 10^{-5}$$

The second order change of the eigenvalue is defined by (2.14) and with $a_{13} = 0$ this yields $d_3 = -0.059$ or by (2.20)

$$(\frac{\Delta\omega_2}{\omega_o})_{theory} = - \frac{d_3}{\lambda_3} = 4.08 \; 10^{-4}$$

The actual experimental values are obtained by fitting parabolae through the spin rates of different 25 minute periods of regular telescope stepping

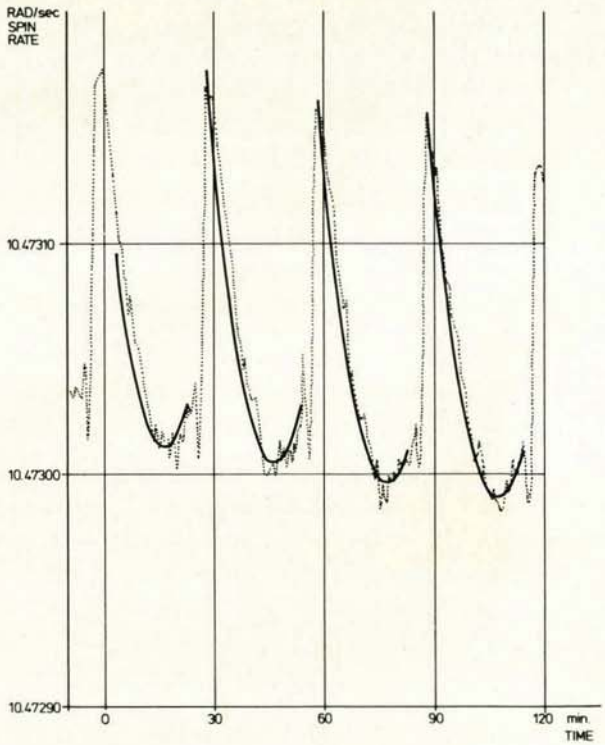

Figure 5

The result is shown in Fig. 5 and is actually the basis of the empiric values. If t is the time in minutes with the origin at 12.5 min away from the scanning mid point, then we find

$$\omega(t) = 10.4703 - 4.338\ 10^{-6}t + 5.01\ 10^{-7}t^2 \quad \text{rad/sec}$$

Transforming t into θ by considering the negative rotation direction

$$t = \frac{-12.5 \times 180}{9 \times} \theta$$

we obtain

$$\left(\frac{\Delta\omega_1}{\omega_o}\right)_{exp} = 3.29\ 10^{-5}$$

and

$$\left(\frac{\Delta\omega_2}{\omega_o}\right)_{exp} = 3.02\ 10^{-4}$$

which is in surprisingly good agreement with the theoretical values.

2.2.2 The Spin axis tilt

For this value we employ the sun colatitude computed for each telemetry format (25.2 sec). To counteract the noise in this case as well, the results of different intervals are superimposed on each other. We further filter the sequences of points by shifting a mean over three consecutive values. The resulting plot is shown in Fig. 6. The sun sensor is at 120° from the spacecraft y-axis and the size of the observed sun colatitude variation appears to be an increase of $5.\ 10^{-3}$ degrees over 25 mins.

From the theory we know that

$$\eta_x = \frac{a_{32}\theta}{\lambda_3 - \lambda_2} = 8.23\ 10^{-3}\ \theta$$

applies to first order. Owing to missing information the second order and η_y cannot be computed at all.

The flight data have been analysed for the month of February where the sun colatitude of METEOSAT 1

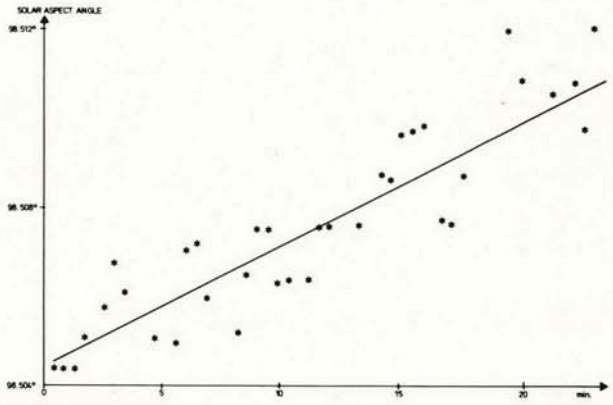

Figure 6

decreases approximately by $1.7\ 10^{-2}$ degrees per 25 mins as for the earth. This should give an increase of sun colatitude only due to tilt equal to $2.2\ 10^{-2}$ degrees. The missing angle η_y prevents us to connect the observed phenomenon to the theoretical values in a coherent manner. Both experiment and theory tend to indicate a larger effect than that which has been reported to us as derived from the earth image analysis.

3. PERIODIC SPIN VARIATIONS UNDER THE INFLUENCE OF THE EARTH

3.1 ESRO IV

3.1.1 The overall spin rate changes

The fact that ESRO IV is a spinning near earth satellite means that the craft is exposed to many different torques affecting both the attitude and the spin rate. The regular eclipses add to this mixture by changing the satellite's temperature in a regular cycle.

A graph showing the observed spin rate changes is added in Fig. 7. This curve shows a smoothed mean

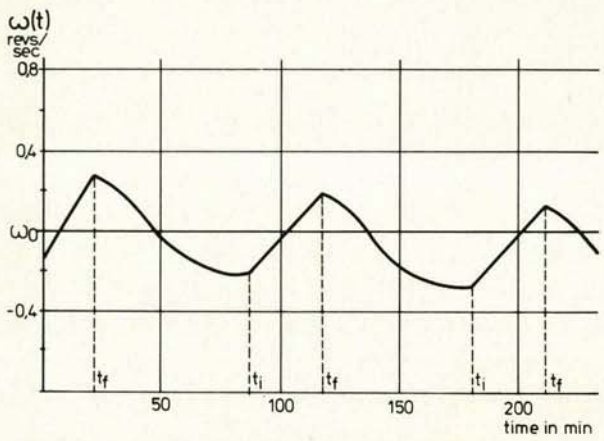

Figure 7

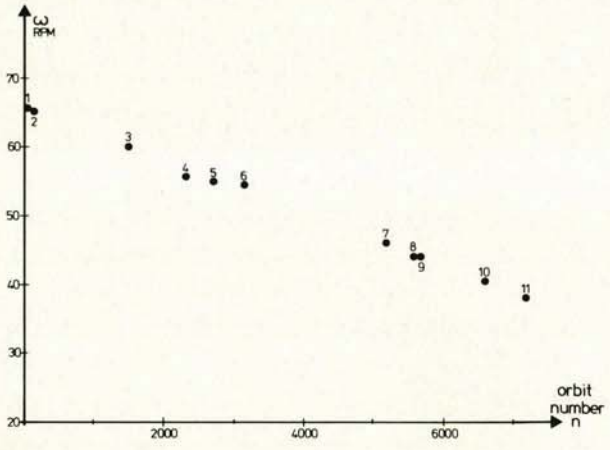

Figure 8

behaviour and the symbols t_i and t_f represent the start and end of eclipse, respectively. The actual spin rate ω can be represented by

$$\omega = \omega_o + \omega_1 t + \Delta\omega(t) \qquad (3.1)$$

where ω_o is a reference spin rate at the selected time original t = 0 and ω_1 is the spin rate decay due to eddy currents. The latter are a function of the inertial attitude of the spacecraft. Indeed, the interaction with the earth magnetic field depends on the relative orientation of the satellite spin axis and the earth magnetic dipole axis. This can be seen on the spin rate decay plot in Fig. 8 where different slopes can be attributed to different attitudes.

The attitude numbering in the figures is chronological. To have an idea about the characteristics of the different attitudes and the external conditions we have compiled table 2. In this table is the earth alignment angle, i.e. the angle between the spin axis of the satellite and the rotation axis of the earth. The angle γ is the sun colatitude or angle between sun direction and the spacecraft spin axis. The ratio t_e/t_p is the fraction of eclipse in the given orbit.

The spin rate decay is not the subject of our interest. The value of ω_1/ω_o has been assessed in ref. 1 and is in the range of $5.5\ 10^{-4}$ to $23.9\ 10^{-4}$ per day. We assume that it is taken out of (3.1), so that we are left with

$$\tilde{\omega} = \omega - \omega_1 t = \omega_o + \Delta\omega(t) \qquad (3.2)$$

or a constant mean spin rate ω_o and a spin rate variation $\Delta\omega(t)$ not due to eddy currents. Buratti and Fusco have called $\Delta\omega(t)$ the 'spin rate anomaly'. It contains a larger periodic part with a period corresponding to the orbital period t_p and a small element $\delta(t,t_p)$. Hence, we have

$$\Delta\omega(t + t_p) = \Delta\omega(t) + \delta(t,t_p) \qquad (3.3)$$

For all the cases investigated, it appears that $\delta(t,t_p) \ll \Delta\omega(t)$ so that we neglect $\delta(t,t_p)$ and concentrate on $\Delta\omega(t)$.

3.1.2 The isolated 'spin rate anomaly'

In Fig. 7 we have seen the periodic character of $\Delta\omega(t)$ which we have expressed in (3.3). Quite naturally, we ask what is the cause of this variation. It can certainly not be generated by either:

- gravity gradient, a magnetic dipole or magnetic fields in the solar array (consisting of 2 independent cylinders with opposite currents) interacting with the earth magnetic field, because the spin motion itself cancels the effect of these torques;

SEQUENCE NR	ORBIT NR	ORBITAL PERIOD MIN	t_e/t_p	ϕ	γ
1	27	99.0	0.155	180°	57°
2	58	98.9	0.197	180°	56°
3	1525	97.7	0.355	125°	114°
4	2335	97.0	0.224	0°	79°
5	2777	96.6	0.195	180°	102°
6	3168	96.3	0.280	180°	100°
7	5267	94.1	0.310	0°	106°
8	5688	93.7	0.225	270°	89°
9	5693	93.7	0.225	270°	90°
10	6667	92.5	0.353	305°	81°
11	7198	91.6	0.388	125°	104°

Table 2 - Synoptic table of ESRO IV attitudes considered in the spin rate analysis

- eddy currents and magnetic hysteresis by varying magnetisation, because these can only spin down the satellite.

The aerodynamic torque however, acts periodically with a maximum at perigee and a negligible effect above 500 km altitude. Though this torque only tends to decrease the spin rate, the removal of all spin decay leaves a periodic spin rate modulation. Thus aerodynamic torques contribute to periodic spin rate changes for satellites on near earth eccentric orbits.

From practical observations we do not see a link of the spin rate temporal evolution with perigee occurence. A verification by Buratti and Fusco shows that

$$\left(\frac{\Delta\omega_M}{\omega_o}\right)_a \simeq 7.5\ 10^{-6} \text{ (orbit 27)}$$

and

$$\left(\frac{\Delta\omega_M}{\omega_o}\right)_a \simeq 2.0\ 10^{-5} \text{ (orbit 7198)}$$

are theoretical values for the relative amplitude of the spin rate modulation due to aerodynamic torques. The notation $\Delta\omega_M$ is for the peak to peak variation of the spin rate. Towards end of life this spin variation represents less than 10% of the total experimental anomaly amplitude.

The conclusion from this analysis is that the thermal behaviour of the total satellite must bring the major contribution to $\Delta\omega(t)$. This is not unexpected. If I_s is the inertia ratio along the spin axis, then in absence of external torques, $I_s\omega$ is constant or

$$\frac{\Delta I_s}{I_s} = -\frac{\Delta\omega}{\omega} \tag{3.4}$$

We can approximate the satellite by a distribution of masses m_i at a distance ρ_{io} from the spin axis with the connecting parts at temperature y_{io}. We assume that only a common temperature gradient Δy affects the inner dimensions. Hence :

$$I_s(y_o) = \Sigma m_i \rho_{io}^2 \tag{3.5}$$

$$\rho_i = \rho_{io}(1 + \zeta\Delta y)$$

where ζ is an equivalent thermal dilatation coefficient. For a change in inertia this yields :

$$\Delta I_s = 2\zeta\Delta y \Sigma m_i \rho_{io} \tag{3.6}$$

By combining (3.4) to (3.6) we obtain

$$\frac{\Delta\omega}{\omega} = -2\zeta\Delta y \tag{3.7}$$

The maximum measured temperature difference (ΔT) at the end of one of the booms is plotted versus

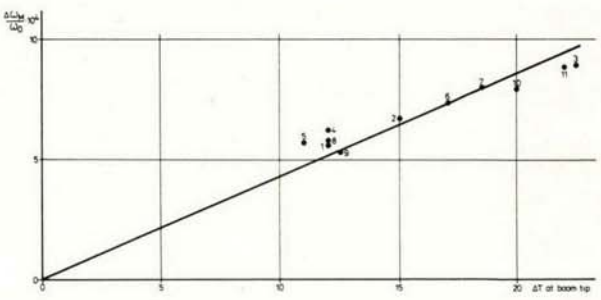

Figure 9

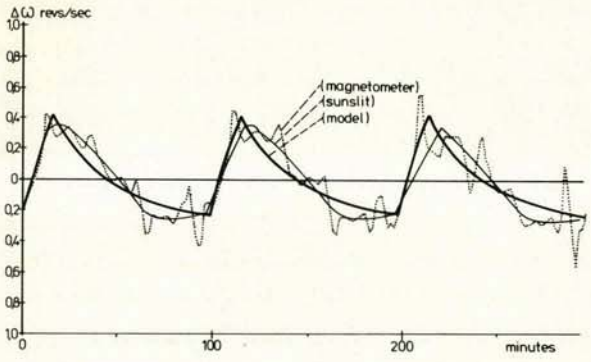

Figure 10

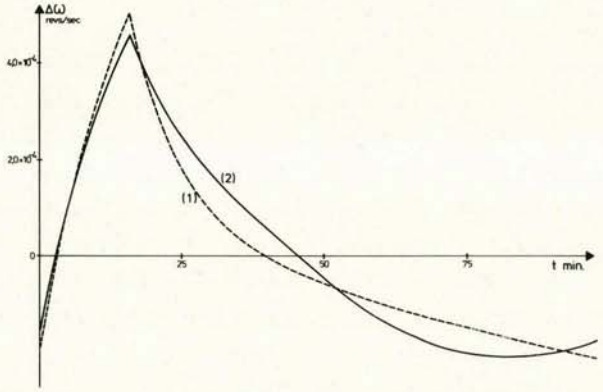

Figure 11

$\Delta\omega_M/\omega$. The linear trend prescribed by (3.7) yields $\zeta = 4.2\ 10^{-5}$ when fitting a straight line to the experimental points. The quality of this linear representation is very good and ζ is close to the dilatation coefficient for aluminium, namely $2.34\ 10^{-5}$.

If we look closer to the curves we discover that the satellite may spin up slightly at the end of this sunlit phase. This is shown for orbits 25 and 26 in Figure 10. The first impression is that (3.7) is too crude and that a more accurate thermal description of the satellite will bring a fully satisfactory fitting between experimental and theoretical results. In the study conducted by A. Buratti and G. Fusco it has been shown that this is not true. The modelling of the satellite into 3 thermal nodes: the interior, the cylinder and the booms, allowing for a realistic thermal coupling amongst them, has not brought the expected fine structure of the simulated behaviour. Pure boom bending or pure boom dilatation had already been excluded as possible candidate causes before.

Just before concluding the study, earth albedo has been introduced as a radiation input over the solar array. In Figure 11, a simulated $\Delta\omega(t)$ is represented for a typical orbit and in :

Case 1 : it contains the thermal model with 3 nodes, coupling between booms and cylinder and a constant albedo input in the sunlit phase at a 30% level of the solar flux.

Case 2 : differs from Case 1 in that the albedo radiation gradually rises from 0% to 30% and decreases back to 0% over a sunlit period.

Obviously this approach is in the right direction. Further investigations could cover :

- modelling of the collected radiation in function of season, latitude and local hour of the sub-satellite point;
- differentiation between earth and solar aspect angles influencing the efficiency of heat collection from both sources.

3.2 METEOSAT 1 Diurnal Spin Modulation

The spin rate of METEOSAT does not only vary with the internal motion of payload parts but it also varies

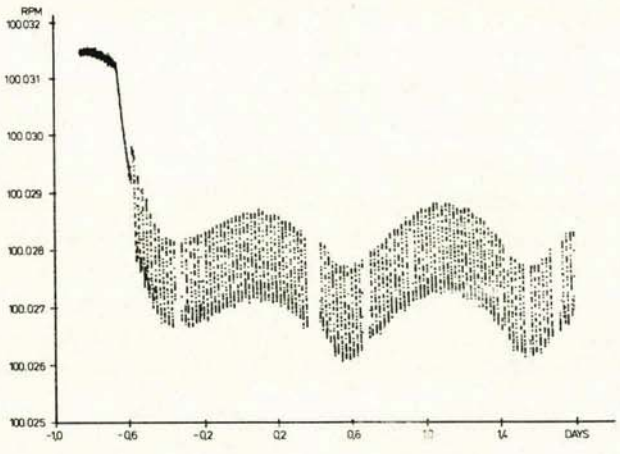

Figure 12

independently from that during the day. As this spacecraft is geostationary, this diurnal variation as shown in Figure 12 is nearly periodic. The abrupt spin down preceeding the daily oscillation corresponds to the 'switch on' of the imaging radiometer. The band of spin rates later on is generated by the telescope motion analysed in section 2. We must remember that the spin axis of this satellite is perpendicular to the orbit plane and hence the solar aspect angle varies from $90^\circ - 23.4^\circ$ to $90^\circ + 23.4^\circ$ and back within one year.

Let us restrict ourselves to the phenomenon inside a day excluding eclipse. Two questions arise : can the magnitude of the variation and the occurrence of minimum spin rate in the afternoon be explained. If we consider the earth albedo as a varying source of energy adding extra electrical power to be dissipated inside the spacecraft, the answer to the previous question is 'yes'.

3.2.1 The Daily Thermal Cycle

Because we are not interested in local temperatures at different positions in the satellite and moreover, the timescale allows for achieving internal thermal equilibrium, we can dispense with conductive and radiative heat transfer inside the body.

The total satellite can thus be approximated by means of a homogeneous cylinder at the absolute temperature y with mass m and specific heat c_p.

If t is time, then the Stefan - Boltzmann equation for radiative heat transfer reads :

$$mc_p \frac{dy}{dt} + \sigma y^4 \Sigma_k \varepsilon_k S_k = \Sigma_k \alpha_k S_k Q_k \qquad (3.8)$$

for all the different boundary surfaces with area S_k. On the left hand side of this equation, we see the change in heat content and the thermal power radiated with emissivity $\varepsilon_k (<1)$ out of the body. On the right hand side we have the thermal power input, where Q_k is the actual thermal power of source 'k' intercepted by the body and α_k is the absorptivity of the body for the arriving radiant power Q_k. Thus $\Sigma(1-\alpha_k) S_k Q_k$ is the amount of power intercepted but rejected by scattering or reflection.

Let us introduce the abbreviations

$$u_{tot} = \frac{\Sigma_k \alpha_k S_k Q_k}{mc_p} \qquad (3.9)$$

and

$$w = -\frac{\Sigma_k \varepsilon_k S_k}{mc_p} \qquad (3.10)$$

The differential equation now looks as follows :

$$y' = u_{tot}(t) + wy^4 \qquad (3.11)$$

The time dependence of $u_{tot}(t)$ needs to be clarified. The integrated spectral power of the sun and the thermal power in the infrared received from the earth nearly remain constant over a day. We denote that part of u_{tot} by u_o. Assuming that the earth atmosphere scatters the albedo equally well also far away from local noon (ref. 4) the radiative albedo power intercepted by the satellite linearly varies during the day.

From local midnight it steadily rises from zero to its maximum at noon and decreases at the same rate in in the local afternoon. We assume that

$$u_{tot} = u_o + vf(t) \qquad (3.12)$$

is a complete representation, where f(t) is periodic function varying from zero to unity.

We display f(t) in figure 13. and define it by

$$\begin{aligned} f(t) &= 2t \qquad 0<t<0.5 \\ f(t) &= -2t+2 \qquad 0.5<t<1 \\ f(t+n) &= f(t) \quad (n=\text{integer}) \end{aligned} \qquad (3.13)$$

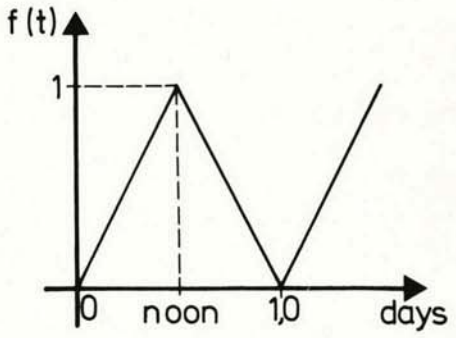

Figure 13

The unit of time is set to one day with the time origin at midnight. The Fourier series representing f(t) is

$$f(t) = 0.5 - \frac{4}{\pi^2} \sum_{k=0}^{\infty} \frac{\cos 2\pi(2k+1)t}{(2k+1)^2} \qquad (3.14)$$

For the purpose of our analysis we can conduct the calculations by only keeping the fundamental frequency in (3.13). This gives the approximate formulation

$$u_{tot} \simeq u_o + 0.5v - \frac{4v}{\pi^2} \cos 2\pi t \qquad (3.15)$$

$$= \alpha + \beta \cos 2\pi t$$

There is of course no hope even with this simplification, to find the integrating factor which should allow an exact integration of (3.11).

Following the method first applied by Fourier himself to the conductive heat equation, we can search for periodic solutions of the non-linear Stefan-Botzmann equation. We assume that a solution represented by a uniformly convergent Fourier series exists. The function y is now defined by

$$y(t) = a_o + \sum_{k=1}^{\infty} (a_k \cos 2\pi kt + b_k \sin 2\pi kt) \qquad (3.16)$$

Again, the harmonics can be left out from our considerations. Indeed, a_1 and b_1 fully define the diurnal spin rate variation and its phase lag with respect to the local day.

We substitute (3.15) and (3.16) in (3.11) and equate the constant and the coefficients of the fundamental terms. This yields after resolution

$$a_o = \left(-\frac{\alpha}{w}\right)^{1/4} \qquad (3.17)$$

$$a_1 = \frac{\beta}{2} \frac{-2wa_o^3}{\pi^2 + 4w^2 a_o^6} \qquad (3.18)$$

$$b_1 = \frac{\beta}{2} \frac{\pi}{\pi^2 + 4w^2 a_o^6} \qquad (3.19)$$

It must be stressed that the values of these terms are not affected by the harmonics of f(t) and that in this respect no approximation is involved.

Let us return to the deeper meaning of y, namely to be the absolute temperature of the body under study. Then $a_o = y_o$, i.e. the mean temperature over the day, and $y_{max} - y_o$ the amplitude of the periodic variation is

$$y_{max} - y_o = \sqrt{a_1^2 + b_1^2} \qquad (3.20)$$

To find the time of minimum temperature t_{min} we introduce ψ by

$$\cos\psi = \frac{a_1}{\sqrt{a_1^2+b_1^2}} \; ; \; \sin\psi = \frac{b_1}{\sqrt{a_1^2+b_1^2}} \qquad (3.21)$$

which allows us to say that

$$y = y_o + \sqrt{a_1^2 + b_1^2} \cos(2\pi t - \psi) \qquad (3.22)$$

The minimum is reached for $2\pi t - \psi = \pi$. If we remember that $w<0$ by (3.10) and $\beta<0$ by (3.15) then we see both a_1 and b_1 are negative and consequently $\pi<\psi<3\pi/2$ holds, or $0<2\pi t_{min}<\pi/2$, i.e. t_{min} is between local midnight and 6 o'clock. The temperature phase lag with respect to periodic heat power input is therefore at most one quadrant.

To gain a better physical understanding in the functional dependencies of y_o, y_{max} and ψ we have to return to the original notations. Making use of (3.10) and (3.15) we find

$$y_o = \left[\frac{(u_o+0.5v)}{\sigma \varepsilon_o} mc_p\right]^{1/4} \qquad (3.23)$$

$$y_{max} - y_o = \frac{2v}{\pi^2}\left[\pi^2 + 4\sqrt{\frac{\sigma\varepsilon_o}{mc_p}(u_o+0.5v)^3}\right]^{-1/2} \qquad (3.24)$$

and

$$tg\psi = \frac{\pi}{2(u_o+0.5v)^{3/4}} \left(\frac{mc_p}{\sigma\varepsilon_o}\right)^{1/4} \qquad (3.25)$$

with $\varepsilon_o = \Sigma \varepsilon_k S_k$

3.2.2 Numerical Application

Let us first define the body which approximates the actual satellite METEOSAT 1. It has the following characteristics :

Cross section $S = 2 \times r \times h = 2 \times 1.05 \times 1.3 = 2.73 m^2$

Mass $m = 280$ kg

Specific heat $c_p = 700$ Joule/(kg grad)

Absorptivity $\alpha = 0.83$; emissivity $\varepsilon = 0.8$

assumed to be constant over the relevant part of the radiation spectrum. The top and the bottom

of the spacecraft are 'superinsulated'. Therefore, we can assume that they only contribute to the mean thermal equilibrium but do not substantially influence the daily thermal cycle of the satellite. Hence, only the satellite cylinder cross-section S projected on a plane perpendicular to the radiation direction has to be considered for radiative input, while the whole cylinder surface participates in the outward radiation.

For the thermal constants we take :

- the Stefan-Boltzmann constant
  $\sigma = 5.67\ 10^{-8}$ Joule/($m^2 grad^4 sec$)
  or in time units of days
  $\sigma = 4.899\ 10^{-3}$ Joule/($m^2 grad^4 day$)
- the total spectral power from the sun $\sim 1358 W/m^2$
- the power in the infrared coming from the earth at geostationary altitude $\sim 5.25 W/m^2$
- the power in the visible (albedo) scattered by the earth is between minimum $k_{min} = 2.28$ and maximum $k_{max} = 9.12$W as received at geostationary altitude above local noon at the equator.

We further have to substract the power radiated out by the radio-communication antenna which a amounts to a constant of 35W.

Changing from seconds to days (factor 86400) yields the following useful quantities

$$\frac{2\pi rh\sigma\varepsilon}{mc_p} = 1.715\ 10^{-7}$$

$$u_o = 1356.4 \sin\gamma - 10.185 \text{ grad/day}$$

where γ is the solar aspect angle. The earth aspect angle is always near 90° and therefore

$$v_i = (k_i . 86400)\ \frac{\alpha S}{mc_p}$$

$$= 0.99889\ k_i \text{ grad/day}$$

The variation shown in Fig. 12 is valid for 8-9 Dec. We want to give a feeling for the values obtained by means of (3.23) to (3.25) if we vary γ. Its value is 90° at equinox and 90 ± 23.4 at solstice. Therefore we have compiled table 3 where $\Delta = y_{max} - y_o$ and t_{lag} is the time lag in minutes derived from Ψ.

EARTH ALBEDO POWER / SUN ANGLE	$v_{min} = 2.28$	$v_{max} = 9.11$
$\gamma = 90^\circ$ $u_o = 1356.4$	$y_o = 297.72^\circ$ K $\Delta = (4.82\ 10^{-2})^\circ$K $\Psi = 199.14^\circ$ $t_{lag} = 76.56$ min	$y_o = 297.91^\circ$ K $\Delta = 0.192^\circ$ K $\Psi = 199.11^\circ$ $t_{lag} = 76.44$ min
$\gamma = 90^\circ \pm 10^\circ$ $u_o = 1335.8$	$y_o = 296.58^\circ$ K $\Delta = (4.87\ 10^{-2})^\circ$K $\Psi = 199.35^\circ$ $t_{lag} = 77.40$ min	$y_o = 296.77^\circ$ K $\Delta = 0.194^\circ$ K $\Psi = 199.31^\circ$ $t_{lag} = 77.24$ min
$\gamma = 90^\circ \pm 20^\circ$ $u_o = 1274.6$	$y_o = 293.10^\circ$ K $\Delta = (5.03\ 10^{-2})^\circ$K $\Psi = 199.99^\circ$ $t_{lag} = 79.96$ min	$y_o = 293.29^\circ$ K $\Delta = 0.201^\circ$ K $\Psi = 199.95^\circ$ $t_{lag} = 79.80$ min

Table 3 : Diurnal thermal variation parameters for METEOSAT 1

For Fig. 12 the solar aspect angle $\gamma \simeq 110^\circ$ applies. The theoretical time lag is some 15 minutes less than the observed phase shift. This is still a good agreement with observations if we consider the level of approximation we have introduced. The theoretical temperature variation has to be cross checked against the spin rate modulation amplitude. We can reuse equation (3.7) to find an equivalent dilation coefficient. If we consider $\Delta\omega/\omega$ to be 1.10^{-5} as can be derived from fig. 12, then we find

$$\zeta\ (v_{min}) = 5.\ 10^{-5}$$

and

$$\zeta\ (v_{max}) = 1.25\ 10^{-5}$$

while ζ for aluminium is $2.34\ 10^{-5}$.

We can conclude that the assumption about the earth albedo is herewith verified to a sufficient extent.

4. SECULAR SPIN RATE CHANGES

The spin rate of GEOS 2 has been the subject of an investigation. We have expected to find a yearly periodic variation. The satellite spin axis is always perpendicular to the earth equator and its solar aspect angle is kept between 65.0° and 90°. To achieve this the spin axis is inverted at each equinox, thus twice a year. A secular variation in the spin rate can be anticipated from the changing solar aspect angle and from the changing sun-spacecraft distance.

The spin rate discontinuously changes at each manoeuvre. When these jumps are eliminated we obtain a steady spin rate increase for which fig. 14 is a typical illustration. The little gaps indicate points where the curves are adjusted to remove abrupt spin rate changes due to manoeuvres. The big jump in September corresponds to the large spin down experienced during the satellite inversion (180° path) at the autumn equinox. The slight change in slope around equinox could be explained by the relatively quick cooling and heating of the satellite especially around the autumn equinox as seen in figure 16. In the mean the spin rate has increased in a uniform manner over the whole life of GEOS 2.

For some satellites such a steady spin rate variation can be so important that it is impossible to overlook. This is the case for the US-spacecraft GOES 1

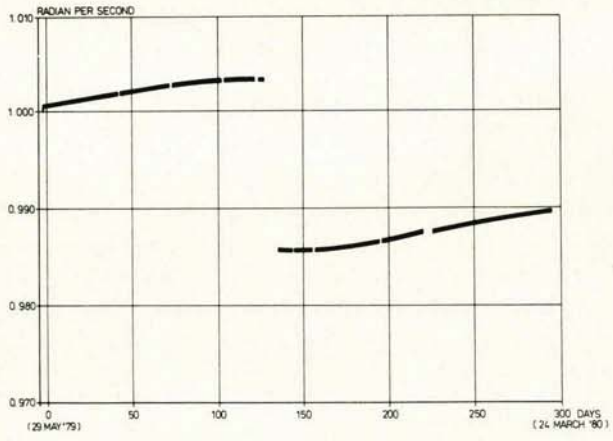

Figure 14

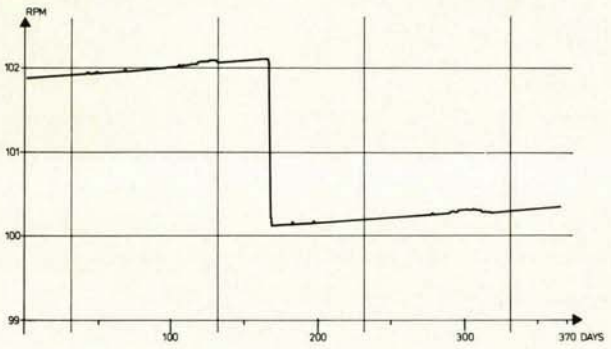

Figure 15

operated by ESOC in 1979 (ref.7) Its spin rate increase is 0.46 rpm/year, as shown in fig. 15. The discontinuity in the month May originates from a spin down manoeuvre.

Other cases often only appear after analysis, such as for the Italian satellite SIRIO 1, (ref. 3) which like GOES 1 and GEOS 1 is a geostationary satellite with its spin axis perpendicular to the equator. This time the spin rate tends to decrease steadily by 0.04 rpm/year.

The three satellites mentioned carry a reaction control system with hydrazine. We quote another example with cold gas thrusters, namely the systematic spin up for HEOS 1 and the monotonic spin down for HEOS 2. Both ESA spacecrafts have flown on highly eccentric orbits with an apogee above 200 000 km. The perigee of these satellites varied between a few hundred to few thousand kilometers under the influence of lunisolar perturbations. A slight spin down by eddy current torques at every perigee passage could have been anticipated. Contrary to this intermittent changes, the in- or decreases have been continuous and in the order of + 0.43 to 2.2 and - 0.18 to - 0.27 rpm/year for HEOS 1 and 2, respectively. The impression gained from these few examples tends to indicate that systematic spin up or down of rigid spin stabilised satellites carrying thrusters is a general phenomenon. That this has not explicitly been observed for many spacecrafts stems from the fact that it is usually a very small effect masked by the spin rate excursions caused by all types of manoeuvres. The attempt to make a statistics over many satellites requires a dispro-

portionate effort. Our intention is to outline a plausible explanation for which we use GEOS 2 as study object. We look for two possible spin rate influences in the long term : one is the yearly thermal cycle which is periodic by it nature, and the other influence is the residual leakage of reaction control thrusters.

4.1 The yearly thermal cycle

From the Stefan-Boltzmann equation in (3.8) we only retain the stationary case. We keep the previous notation except for the thermal power input which we write now as p(t). The equation reads

$$y^4(t) = \frac{p(t)}{\sigma \sum_i \varepsilon_i S_i}$$

The time dependence of p(t) is governed by the change in solar radiation power k(t) received per unit area (ellipticity of the earth orbit) and the variation of the solar aspect angle γ (t). If t is the time in calendar years with the origin at 0 January, we know that

$$k(t) = 1358.(1.0004 + 0.03348 \cos 2\pi\ (t-0.502))^{-1} \qquad (4.2)$$

For $\gamma(t)$ the behaviour of fig. 13 applies. The minimum, i.e. $\gamma = 66.5^\circ$ is reached at solstice and rhe maximum, i.e. $\gamma = 90^\circ$ at equinox. This is shown by the dotted line in Figure 16.

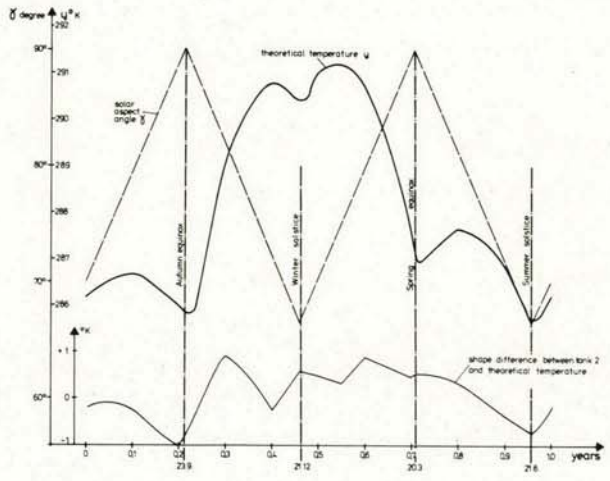

Fig. 16

The satellite as a whole is approximated by a homogeneous cylinder with the following mean characteristics :

- r radius of the cylinder : 0.822 m
- h height of the cylinder : 1.175 m
- α_c absorptivity of the cylindrical surface: 0.83
- ε_c emissivity of the cylindrical surface: 0.80
- α_b top and bottom absorptivity : 0.2 and ε_b, the emissivity for top and bottom is equal to α_b

The input radiative power now becomes

$$p(t) = k(t) \left\{ 2rh\alpha_c \sin\gamma\ (t) + \pi r^2 \alpha_b \cos\gamma(t) \right\} \qquad (4.3)$$

and further

$$\sum_k \varepsilon_k S_k = 2\pi rh\varepsilon_c + 2\pi r^2 \varepsilon_b \qquad (4.4)$$

Working out (4.1) by means of this information yields the behaviour of y, the absolute temperature, as a function of the time of the year. This is shown in fig. 16. Neglecting the top and the bottom of the satellite should give rise to a temperature minimum at the solstices and a maximum at the equinoxes. We have compared our results with the most stable inner temperature reported for GEOS 2, namely that of the hydrazine tank number 2. Apart from a mean constant difference of 5°, the temporal evolution of our result coincides within $\pm\ 1^\circ$ with the observed temperature. We are not really interested in the mean temperature but in its peak to peak amplitudes over the year. We take the experimental value of 6.5° which is 1° smaller than what the approximate calculation yields.

To compute the effect on the spin rate we again use (3.7), or

$$\frac{\Delta\omega}{\omega} = -2\zeta\ \Delta_y \qquad (4.5)$$

where this time $\zeta = 2.35\ 10^{-5}$, $\Delta y = 6.5$ and $\omega = 10$ rpm are given. The maximum spin rate change for the yearly thermal cycle of GEOS 2 is $3.06\ 10^{-3}$ rpm.

Compared to the diurnal variation studied for METEOSAT 1, the yearly variation is an order of magnitude higher for both temperature and spin rate. Neverthe-

less it is too small by a factor of 20 when looking at figure 14. The main part of the secular spin rate change does thus not come from the yearly thermal cycle.

4.2 Torques from residual thruster leakage

We know that in ESA hydrazine thrusters are tested and qualified for leakage rates of 1 to 3 standard cm^3/hr of helium or nitrogen under 1 atmosphere at 0^o celsius. For a liquid like hydrazine this can be considered as hermetically closed from an engineering standpoint, though it does not exclude the leakage of some grams per year. Moreover, if we loose less than 1 kg of fuel over the total lifetime of a satellite we will hardly realise it, especially if we consider all inaccuracies playing a role in fuel budgetting. We have thus to verify whether the amounts of fuel required to cause the observed spin up or down are in an acceptable order of magnitude to fit in the context of thrusters qualification level and fuel budget observability limits. Assume that n_s is the component of a torque along the spin axis, then a spin rate change of size $\Delta\omega$ is given by

$$\Delta\omega = \frac{n_s}{I_{spin}} \Delta t \qquad (4.6)$$

when the torque acts during a time Δt. Formula (4.6) is valid for symmetric bodies and also if n_s is so small that dynamical coupling can be neglected for asymmetric bodies like GEOS 2.

If l is the lever arm of a thruster, ϕ its cant angle with respect to a tangential to a cylinder around the spin axis, v the speed of the escaping gas molecules and m_g the mass of the outflowing fuel, then

$$n_s = lvm_g \cos \phi \qquad (4.7)$$

or by substitution in (4.6)

$$m_g = \frac{I_{spin}}{lv \cos \phi} \frac{\Delta\omega}{\Delta t}$$

For GEOS 2 we can hypothize that the tangential spin up thruster ($\phi = 7^o$) with a lever arm of 0.8 m is giving rise to the systematic spin rate change If v is 2 km/sec then

$$m_g = \frac{4o4.5}{0.8 \times 2. \ 10^3 X 0.993} \left(\frac{4. \ 10^{-3}}{150}\right)$$

$$= 6.79 \ 10^{-5} \text{ kg}$$

is lost in a day, or 2.48 gr/year. Of course, this is only the net resultant of different leakages. If we now assume that each thruster leakes and loses say 1.5 gr per year it is clear that altogether we will never measure this in the fuel budget. Considering the spin motion, the overall small velocity increment will always be along the spin axis . Because such forces act during the whole orbit, at least geostationary satellites will not experience secular orbit influences by thruster leakage.

For GOES 1 we have performed a similar verification and find a fuel loss of 19.5 gr per year only for the net resultant spin up torque. For SIRIO 1 a fuel loss of 180 gr/year has been reported in in ref. 3. In the case of SIRIO 1 the leakage comes from misaligned radial and axial thrusters and the systematic spin decay has not been constant over the years. For GEOS 2 the constancy of spin up in between many manoeuvres is remarkable just like for GOES 1. This may suggest that thrusters no longer used after initial station acquisition remain leaking at a relatively constant rate.

5. CONCLUSIONS

5.1 The Order of Magnitudes

In this paper we have amongst others established the size of different effects on the spin rate ω. Before summarising these results let us repeat the definition of the dimensionless relative spin variation: -

$$\frac{\Delta\omega}{\omega} = \frac{\omega_{max} - \omega_{min}}{\omega_{mean}}$$

Clearly, the slow motion of internal parts change the spin rate in proportion to the masses involved. A careful design can reduce the influence on the spin rate but the design optimisation should not go beyond the small spin variations which will occur for physical reasons anyway.
The hierarchy of relative spin variations observed and and explained is as follows : -

- near earth orbital missions with eclipse : $\omega = \Delta\omega$ 1. 10^{-3} periodic, temperature range Δy = 10^{o} to 20^{o};

- thruster leakage at least 5. 10^{-2} and up to 0.5 rpm/year;

- thermal yearly, geostationary missions : $\omega = \Delta\omega$ 1.5 10^{-4} periodic, temperature range Δy = 5^{o} to 10^{o}

- diurnal albedo, geostationary missions : $\omega = \Delta\omega$ 1. 10^{-5} periodic, temperature range $\Delta y < 0.5^{o}$.

These figures should be understood as engineering order of magnitudes.

5.2 The Theoretical Background

Especially for the telecope motion inside METEOSAT 1 the theory fits the actual flight data better than previous studies. This good agreement has been achieved by :

- the careful dynamic analysis;
- the original part on eigenvector and eigenvalue approximation.

For the relative spin variations caused by changes of the mean satellite temperature Δy the following formula: -

$$\frac{\Delta\omega}{\omega} = -2\zeta\Delta y$$

appears to be a very powerful approximation. We recall that ζ is the dilatation coefficient of aluminium and thus $\zeta = 2.3\ 10^{-5}\ grad^{-1}$.

5.3 Spin Control

In all the cases we have studied it would have been difficult to predict the relative spin variations before launch very accurately. For those missions where the exact spin rate size and its control play an important role, the 'in-flight' calibration seems mandatory, especially as we do not know beforehand how large the 'leaking thruster effect' will be.

We have paid little attention to abrupt power dissipation changes. In figure 12 we find an example where this gives rise to $\Delta\omega = 5.\ 10^{-5}\ \omega$ in less than half an hour, i.e. five times the diurnal variation. Thus, in the cases we want to steer the spin rate very accurately, open loop ground control is unavoidable.

6. REFERENCES

1. Buratti A. und Fusco G., 'Investigation on spin rate fluctuations of the ESRO IV satellite', ESOC study contract 626/74/AR, C.I.A., Rome 1975.

2. Brunet P., 'Perturbation de la stabilisation du satellite par le basculement du telescope', Doc. nr. 84/85 TDA rev A, SNIAS, Cannes 1979

3. De Agostini A., 'SIRIO-1 spin phase determination and prediction', DPS-TES-NT/1412.02/260381, Telespazio, Rome 1981

4. Howell J.R. and Siegel R., 'Thermal radiation heat transfer', NASA SP-164, Vol I sect. 5 , Washington 1969

5. Kato T., 'Perturbation Theory for linear operators', Springer Verlag, Berlin 1966

6. Kohler P., 'High accuracy observation and model for the spin rate of a geostationary satellite', OAD working paper 113, ESOC, Darmstadt 1978

7. Laue H., editor,'GOES 1.0 Operational mission', Flight Dynamics Report, ESOC, Darmstadt 1980

8. Lebegue, 'Qualité Image, Dossier des etallonages relatifs à F1 nécessaires au segment sol pour le traitement des Images', Doc. Nr. 2362/85TKA, SNIAS, Cannes 1977

9. Wittenburg J., 'Dynamics of systems of rigid bodies', B.G. Teubner, Stuttgart 1977.